Experimental validation of TNO trailing edge noise model and application to airfoil optimization

Bertagnolio, Franck; Aagaard Madsen, Helge; Bak, Christian

Published in:
EWEC 2009 Proceedings online

Publication date:
2009

Document Version
Publisher's PDF, also known as Version of record

Experimental Validation of TNO Trailing Edge Noise Model and Application to Airfoil Optimization

Franck Bertagnolio[*,+]**, Helge Aa. Madsen**[*]**, and Christian Bak**[*]

[*] Wind Energy Division
National Laboratory for Sustainable Energy
Risø DTU, Technical University of Denmark
P.O. Box 49, DK-4000 Roskilde - Denmark

[+] E-mail: franck.bertagnolio@risoe.dtu.dk
Tel.: (+45) 4677 5088 Fax: (+45) 4677 5083

Abstract: The first part of this study is aimed at validating a trailing edge noise model by comparison with experimental data. Measured airfoil surface pressure fluctuations are compared with the component of the model that relates the turbulent boundary layer characteristics to the surface pressure. Far field sound pressure levels are also considered for comparisons between model results and experimental data.

In the second part, the model is implemented into an airfoil design code that is normally used for aerodynamic optimization. An existing wind turbine airfoil is optimized in order to reduce its noise emission, trying at the same time to preserve its aerodynamic performances. The modifications resulting from this new design are analyzed.

1 Introduction

In order to increase public acceptance of wind turbines, there is a strong need to reduce their noise emission. There is a general agreement that one of the main sources of noise originates from the scattering of aerodynamic noise at the trailing edge of the blades.

There exist various models that can be used to predict the acoustic noise radiated from an airfoil trailing edge [1, 2, 3]. In the present study, the so-called TNO model [4] based on a solution of the turbulent boundary layer pressure field giving access to the airfoil surface pressure near the trailing edge is considered. Theoretical work synthetized by Blake [5] is used as a foundation to formulate this solution. From there, it is possible to express the acoustic noise scattered by the trailing edge in the far field using a theory originating from the works of Ffwocs-Williams and Hall [6]. It was subsequently improved by various authors as summarized and unified by Howe [7].

As input, the previous model requires a description of the turbulent boundary layer near the airfoil trailing edge. For example, a panel method coupled to an integral boundary layer formulation as in the software XFOIL [8] can be used. Alternatively, any Computational Fluid Dynamic (CFD) code including a turbulence model for the boundary layer can be considered. In this paper, both XFOIL and CFD calculations will be used for the model validation. However, only XFOIL will be used for airfoil optimization in Section 3 since it is considerably less computationally expensive. This is indeed an important issue for airfoil optimization that typically requires a large number of cost function evaluations, each of these usually requiring several flow field calculations.

The aim of this work is two-sided. Firstly, wind tunnel measurements of airfoil surface pressure are used to validate the surface pressure prediction part of the aeroacoustic model. Experiments for which far field noise has been measured are presented as well and sound pressure level spectra are compared with the model results. Secondly, this study is concerned with the optimization of a wind turbine airfoil in order to reduce its trailing edge noise emission. The noise model introduced above is implemented in an in-house airfoil design code and noise-optimized airfoil designs subject to various geometric and aerodynamic constraints are proposed. The results of this design process are analyzed.

2 Validation of a Trailing Edge Noise Model

In this section, the formulation of the trailing edge noise model that will be used in the remaining of this paper is presented. Measurements are used to validate the two components of the model: pressure spectra on the airfoil surface and far field noise Sound Pressure Levels (SPL).

2.1 The TNO Model

This model originally proposed by Parchen [4] is gathering several results from previous studies. These are used to formulate a far field noise SPL expression as a function of turbulent boundary layer characteristic quantities.

In more detail, the first part of the model is based on a formula expressing the contribution of the mean-shear/turbulence interaction in the boundary layer, which relates the turbulent boundary layer characteristic quantities to the fluctuating surface pressure (see Blake [5], Vol.II, pp.513-524). Manipulating the previous formula, Parchen [4] arrived to the following result for the wavenumber-frequency surface pressure spectrum:

$$\Phi_p(\boldsymbol{k},\omega) = 4\rho_0^2 \frac{k_1^2}{k_1^2+k_3^2} \int_0^{+\infty} L_2(y_2)\,\overline{u_2^2}\left(\frac{\partial U_1}{\partial y_2}(y_2)\right)^2 \Phi_{22}(\boldsymbol{k}) \times \Phi_m(\omega - U_c(y_2)k_1)\,\mathrm{e}^{-2|k|y_2}\,\mathrm{d}y_2 \quad (1)$$

where the subscripts $1, 2, 3$ denote directions parallel to the airfoil surface in the main flow direction, perpendicular to the surface, and along the trailing edge, respectively, $|k|$ is the norm of the 'surface' wavenumber $\boldsymbol{k} = (k_1, 0, k_3)$, ω is the circular frequency, ρ_0 is the density, L_2 is the vertical integral length that characterizes the vertical extent of the turbulent eddies, $\overline{u_2^2}$ is the vertical velocity Reynolds stress component assumed proportional to the turbulent kinetic energy k_t, U_1 is the streamwise mean velocity (its derivative, the mean shear, actually appears in the integral), Φ_{22} is the spectrum of the vertical velocity fluctuations (modelled using the classical Von Karman theory), Φ_m is the so-called moving axis spectrum that describes how Φ_{22} is distorted by the generation and destruction of eddies during their convection past the trailing edge, and U_c is the convection velocity of these eddies. The various quantities involved in the previous formula can be deduced from the fluid flow solver (such as the velocity profile), or from theoretical results (usually assuming isotropy), or a combination of both. Turbulent kinetic energy is directly available from a CFD code or can be related to the mean shear [9] if using XFOIL. As for the integral length scale, the approach followed by Lutz *et al* [10] is implemented when using CFD, otherwise it is determined using Prandtl theory [9]. The remaining quantities are defined as specified in the model implementation by Moriarty [9]. Note that the surface pressure frequency spectrum is obtained from Eq.(1) by integrating over the whole surface wavenumber space and reads:

$$\Phi_{\text{surf}}(\omega) = \iint_{-\infty}^{\infty} \Phi_p(\boldsymbol{k},\omega)\,\mathrm{d}k_1\mathrm{d}k_3 \quad (2)$$

The second part of the model consists in expressing the far field noise as a function of the previous wavenumber-frequency spectrum of the surface pressure fluctuations. Using the formula of Brooks and Hodgson [11], the far field pressure spectrum density can be expressed as an integral of the wall pressure spectrum over the wavenumber component in the flow direction:

$$S(\omega) = \frac{L}{4\pi R^2} \int_{-\infty}^{+\infty} \frac{\omega}{c_0 k_1} \Phi_p(\boldsymbol{k},\omega)|_{k_3=0}\,\mathrm{d}k_1 \quad (3)$$

where R denotes the distance from the trailing edge to the observer (located 90^o with respect to the main flow direction above the trailing edge), L the span extent of the trailing edge, and c_0 is the speed of sound.

In this section, CFD calculations are performed with the in-house two-dimensional incompressible Navier-Stokes solver EllipSys2D. The $k-\omega$ SST model by Menter [12] is used as a turbulence model. The reader is refered to previous publications for more details about this code [13, 14].

2.2 Surface Pressure Validation in LM Wind Tunnel

The NACA0015 was equipped and measured in the LM Glasfiber wind tunnel, which is specifically designed for the aerodynamic testing of wind turbine airfoils. In the absence of turbulence grid (as it is considered herein), a previous study has shown that turbulence intensity in the incoming flow is of the order of 0.1% at all speeds [15]. The airfoil section was instrumented with an array of high-frequency microphones mounted beneath its surface. The microphone the most downstream on the airfoil surface located at a non-dimensionalized distance from the trailing edge equal to $x/C = 0.567$ is considered here only.

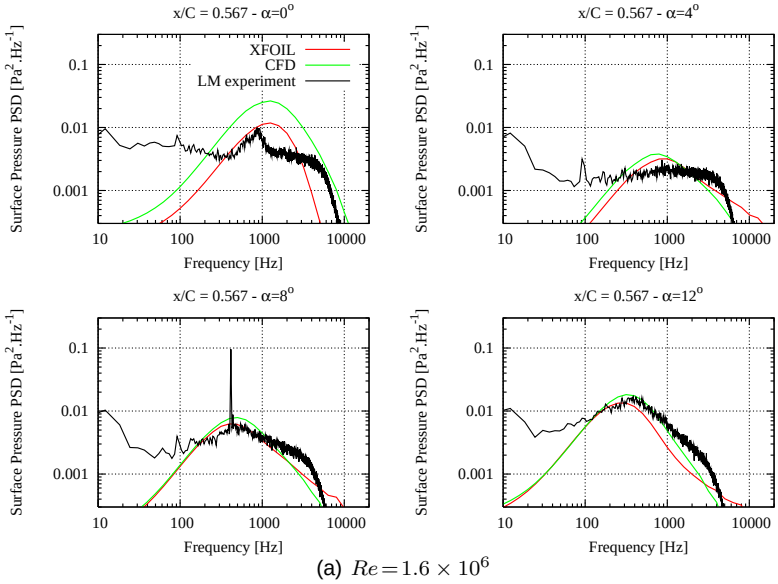

(a) $Re = 1.6 \times 10^6$

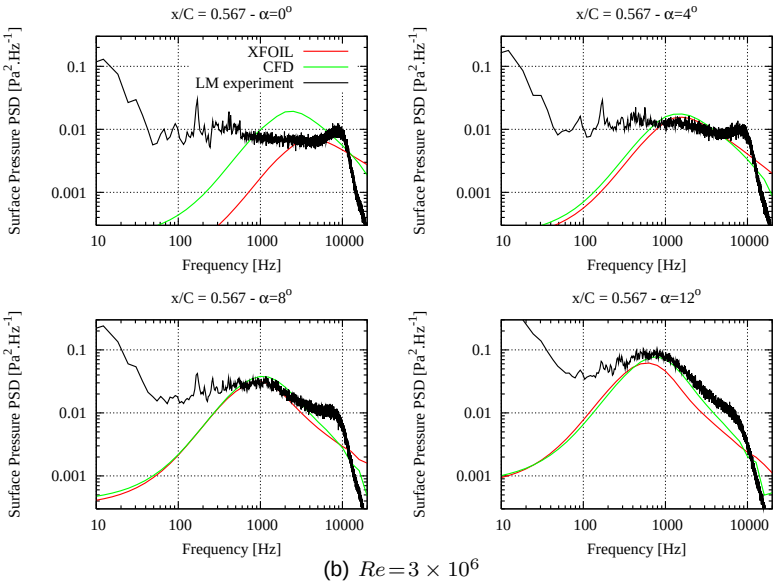

(b) $Re = 3 \times 10^6$

Figure 1: Surface Pressure Spectra on NACA0015 Airfoil at Various Angles of Attack

Measurement results at two inflow velocities, resulting in Reynolds numbers equal to $Re = 1.6$ and 3×10^6, and at various angles of attack ($\alpha = 0, 4, 8, 12^o$) are presented. These are compared with results obtained with the TNO model using Equation (2) and for which the flow field is computed either with XFOIL or the CFD code EllipSys2D. Figures 1(a) and (b) show the surface pressure spectra for the two Reynolds numbers, respectively, for increasing angles of attack. It can be seen that at angle of attack $\alpha = 0^o$, the model results diverge noticeably from measurements. This is due to the fact that the turbulence transition is located quite close upstream the measurement point $x/C = 0.567$. The assumption of fully developed turbulent boundary layer does not hold here and this results in a surge of pressure fluctuations in this region. This feature was also observed in experimental data [16]. At higher angles of attack, transition occurs closer to the leading edge and is not felt at the measurement point. Indeed, the numerical results reproduce quite well the increase in power spectral density in the frequency range $300 < f < 9000$ Hz as the angle of attack increases. However, the TNO model does not capture the lower frequency part of the measured spectra. It is probable that these frequencies are dominated by additional sources originating from flow conditions or various perturbating effects (acoustic reflections, etc...) in the wind tunnel, which is not designed for aeroacoustic measurements. In addition, the Von Karman

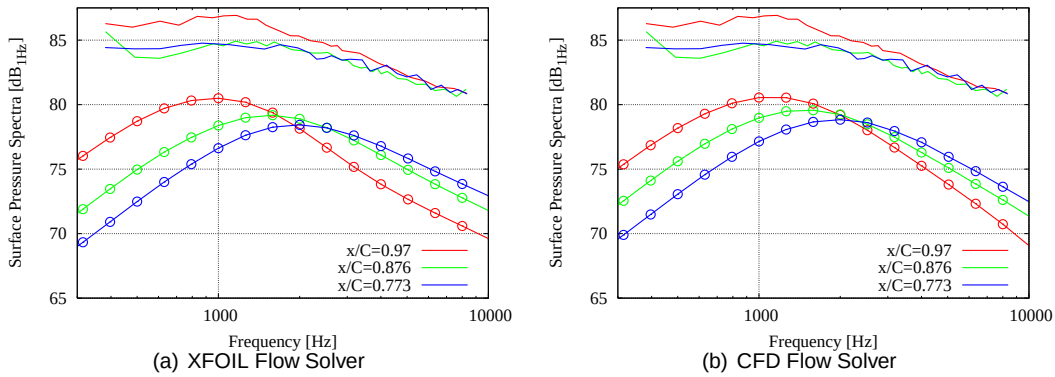

(a) XFOIL Flow Solver (b) CFD Flow Solver

Figure 2: Surface Pressure on NACA0012 Airfoil (Lines: Experiment [11]; Lines with points: TNO model)

spectrum used in the model is usually a poor estimation at low frequencies where these particular flow characteristics dominate. It should finally be noted that the CFD flow calculations perform slightly better than XFOIL for higher frequencies.

2.3 NACA0012 Airfoil Measurements at NASA Langley

The measurements performed by Brooks and Hodgson [11] in the anechoic quiet flow wind tunnel facility at NASA Langley Research Center are now reported. The considered airfoil is the NACA0012 airfoil section with a sharp trailing edge and a chord $C = 0.6224$ m. Inflow velocities are equal to 38.6 and 69.5 m/s resulting in Reynols numbers equal to $Re = 1.6$ and 2.9×10^6. Two angles of attack are considered: $\alpha = 0$ and 5^o.

A series of pressure sensors were mounted on the airfoil surface at various distances from the trailing edge. In addition, microphones located in the plane perpendicular to the midspan section of the airfoil are used to measure the trailing edge far field noise.

In a first place, the measured surface pressure spectra for $Re = 2.9 \times 10^6$ and $\alpha = 0^o$ are compared with TNO model results using XFOIL and EllipSys2D calculations in Figs.2(a) and (b), respectively. In these figures, three surface pressure sensor locations are considered: $x/C = 0.773, 0.876$ and 0.97. An offset between 5 and 10 dB is observed between the measurements and the model results. Despite checking our method for errors and dimensionalizing factors, there could exist an inconsistency between our formulation and the one used in Brooks and Hodgson [11]. Alternatively, it could be that the TNO model predicts too low pressure values. Nevertheless, an inconsistency in conventions cannot be ruled out since the model results did match quite well measurements in Section 2.2. In any case, it can be seen that both flow calculation methods reproduce the same tendencies as the measurement data. Indeed, the pressure spectral density increases as the trailing edge is approached and the peak frequency decreases at the same time.

In a second place, far field SPL are displayed in Figs.3(a) and (b) for angles of attack $\alpha = 0$ and 5^o, respectively. As previously, an offset in pressure levels is observed. However, taking this offset aside, the measurement data tendencies relatively to the varying inflow velocity are well reproduced by the model. The spectrum peak frequency is slightly underestimated by the model in particular for XFOIL calculations at $\alpha = 5^o$.

2.4 NACA0012 Airfoil in the Aeroacoustic Windtunnel Braunschweig

The NACA0012 airfoil was also measured in the Aeoroacoustic Windtunnel Braunschweig (AWB) facility at the Institute für Aerodynamik und Strömungstechnik (DLR) [17]. The acoustic measurement device consists of an elliptic mirror system. The considered measurements involve the 0.4 m chord airfoil at zero angle of attack and for wind speeds equal to 40, 50 and 60 m/s.

Far field SPL at $\alpha = 0$ are displayed in Figs.4(a) and (b) using XFOIL and EllipSys2D, respectively. As in the previous section, an similar offset in SPL is observed. Nevertheless, the model reproduces the tendencies of the measurements (increase in SPL and shifting to the right of the spectrum peak frequency) with respect to increasing velocity.

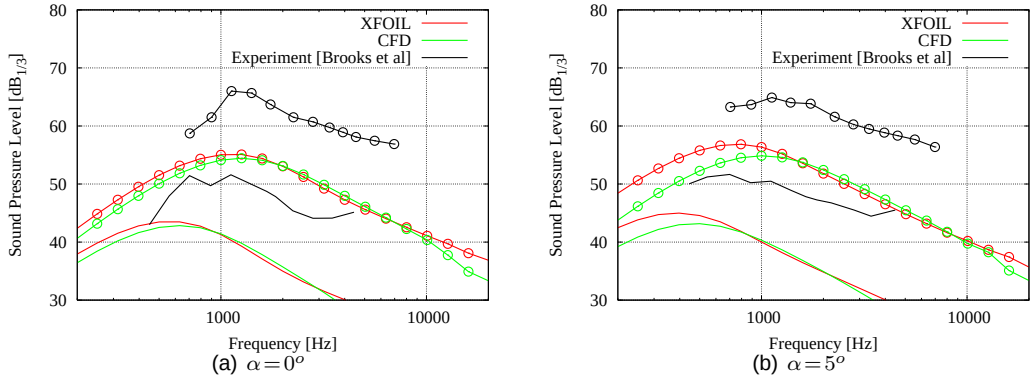

(a) $\alpha = 0^o$ (b) $\alpha = 5^o$

Figure 3: Far Field SPL for NACA0012 Airfoil (Lines: $U = 38.6$ m/s; Lines with points: $U = 56.5$ m/s)

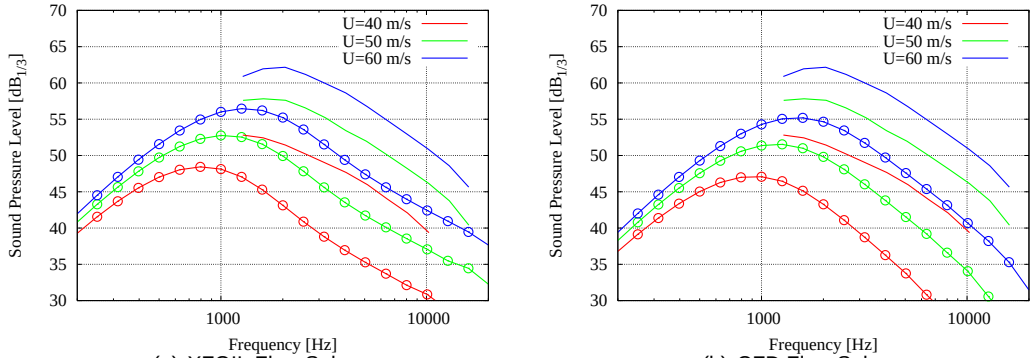

(a) XFOIL Flow Solver (b) CFD Flow Solver

Figure 4: Far Field SPL for NACA0012 Airfoil (Lines: AWB Experiment [17]; Lines with points: TNO model)

2.5 Discussion

In this section, various measurements data were compared with the TNO trailing edge noise model using both XFOIL and CFD calculations. In some cases, the quantitative agreement between the experimental data and calculations results was quite poor. In particular, it seems that the TNO model (with this present implementation) predicts in some cases too low pressure levels (both surface pressure and far field SPL) compared to measurements. This was however also observed in other studies by various authors [18, 19]. Results obtained with the CFD flow solver proved in most cases to give results slightly closer to experimental data compared to XFOIL calculations.

Nevertheless, all these comparisons indicate that the TNO model is capable of reproducing the tendencies observed in measurements independently of the flow solver. Therefore, this model is a good candidate for implementation in an airfoil design code since optimization algorithms are based on relative improvements from one particular airfoil to the other and not on quantitatively accurate results.

3 Airfoil Aeroacoustic Optimization

In this section, the TNO model is implemented into an optimization program that is originally used for airfoil aerodynamic design. Our goal is now to improve the acoustic properties of a given airfoil.

3.1 The Optimization Program *AirfoilOpt*

The optimization code *AirfoilOpt* is an airfoil/blade section profile design tool that was developed at Risø National Laboratory [20, 21]. It is based on a so-called Sequential Linear Programming technique to reduce a given cost function subject to various constraints. In short, for a given set of design parameters, at each iteration of the numerical procedure the code calculates the

local gradients of the cost function associated to each parameter in order to find a new iterate improving the value of the cost function. This cost function can be a linear combination of various geometric (surface curvature, camber, thickness distribution, etc...) or aerodynamic (lift, drag, moment coefficients, lift/drag ratio, transition location, etc...) characteristics of the airfoil section. The aerodynamic data are computed with the airfoil analysis code XFOIL by Drela [8]. In addition, non-linear constraints on the geometric and aerodynamic properties of the airfoil can be enforced during the optimization process. Note that the cost function and constraints may involve aerodynamic characteristics of the airfoil calculated both using fully turbulent flow conditions and transition modelling in the flow solver.

As part of the present work, the original optimization code has been extended by introducing trailing edge noise as a possible component of the cost function or constraints. In this study, the maximum value of the non-filtered far field SPL spectrum across the whole frequency range is used as the cost function. It was found in a preliminary study that A-weighting alters the convergence of the optimization algorithm by smearing out the cost function gradients. Both the pressure and the suction side noise spectra are considered and added to each other. However, only the suction side generated noise will be of interest for the flow conditions that we are interested in. In addition, it was found that including other aerodynamic quantities in the cost function also yields to convergence problems. However, in order to preserve some of the aerodynamic properties of the reference airfoil, constraints on the aerodynamic quantities will be enforced during the optimization process.

In the following of this section, the RISØ-B1-18 is considered as the reference airfoil. The SPL in the cost function is evaluated at the single angle of attack $\alpha = 6^o$. It must be noted that for each optimization calculation, the iterative procedure is started from the original reference airfoil. All calculations are pursued until a local optimum for the cost function is reached.

3.2 RISØ-B1-18 Airfoil

The RISØ-B1 airfoil family was designed for use on MW-size wind turbines with variable speed and pitch control [22]. It was designed to have high maximum lift and high design lift and allow a slender flexible blade while maintaining high aerodynamic efficiency. Only the airfoil with 18% thickness-to-chord ratio is considered here.

As a first step, a new airfoil is acoustically optimized so that the geometric and aerodynamic design properties of the original RISØ-B1-18 are preserved by using constraints. This set of constraints, refered to as "*All constraints*", involves in particular the airfoil shape and thickness distribution in relation with fabrication constraints, transition location, aerodynamic performances at stall and in deep stall. Those relevant for the present study read:

- Geometric constraints:
  - On the suction side: $y_{,xx}(0.4 < x < 0.9) < -0.15$
    $0.28 < x(y_{\text{max}}) < 0.35$
  - On the pressure side: $y_{,xx}(0.7 < x < 0.9) > -1.1$
    $0.28 < x(y_{\text{min}}) < 0.35$

- Aerodynamic constraints:
  - Maximum lift: $1.825 < C_l(\alpha_0 = 17^o)$
  - Lift beyond stall: $1.69 < C_l(\alpha_0 = 22^o)$
    $1.66 < C_l(\alpha_0 = 24^o)$
    $1.63 < C_l(\alpha_0 = 30^o)$

where x denotes the chordwise coordinate non-dimensionalized with the airfoil chord and which origin is at the trailing edge. The airfoil shape is then defined by $y(x)$, the vertical distance to the chord axis. $y_{,xx}$ denotes the second order derivative of the airfoil shape relatively to the chordwise coordinate, also denoted as curvature. $x(y_{\text{min}})$ and $x(y_{\text{max}})$ denote the chordwise locations of the minimum and maximum values of y on the airfoil profile. The lift coefficient C_l is defined as a function of the angle of attack relative to zero-lift α_0. All the previous aerodynamic constraints (except the one concerning transition location) are enforced for fully turbulent flow conditions.

3.3 Relaxed Geometric and Aerodynamic Constraints

The geometric constraints that were enforced above can be relaxed in order to widen the feasible design space and further reduce trailing edge noise. Two different designs are proposed. Preserving all the remaining constraints present in the "*All constraints*" design introduced above, the two designs are obtained by modifying only the following constraints:

- Design "$y_{\text{min,max}}$"
  On the suction side: $0.23 < x(y_{\text{max}}) < 0.40$
  On the pressure side: $0.23 < x(y_{\text{min}}) < 0.40$

- Design "$y_{,xx}$"
  On the suction side: $y_{,xx}(0.4 < x < 0.9) < -0.12$
  On the pressure side: $y_{,xx}(0.7 < x < 0.9) > -1.3$

The results of these design constraints after optimization, namely the airfoil shapes, lift-drag characteristics and SPL spectra, are displayed in Figs.5(a), 6(a) and 7(a). It can be seen that the best noise reduction is obtained with the "$y_{\text{min,max}}$" design, yielding also the largest change in airfoil shape. All designs yield similar aerodynamic characteristics.

The aerodynamic constraints are now relaxed. As in the two previous designs, all remaining constraints of the "*All constraints*" design remain unchanged. Two designs are proposed with the following modified constraints:

- Design "C_l *beyond stall*"
  Lift beyond stall: $1.59 < C_l(\alpha_0 = 22^o)$
  $1.56 < C_l(\alpha_0 = 24^o)$
  $1.53 < C_l(\alpha_0 = 30^o)$

- Design "*All* C_l"
  Maximum lift: $1.725 < C_l(\alpha_0 = 17^o)$
  Lift beyond stall: $1.59 < C_l(\alpha_0 = 22^o)$
  $1.56 < C_l(\alpha_0 = 24^o)$
  $1.53 < C_l(\alpha_0 = 30^o)$

Airfoil shapes, lift-drag characteristics and SPL spectra after optimization are displayed in Figs.5(b), 6(b) and 7(b). All designs yield similar noise reductions and aerodynamic characteristics indicating that lift constraint in deep stall is the main parameter for noise reduction. Indeed, even when relaxed, the lift at stall is not modified.

Note that the RISØ-B1 airfoil series is proprietary and therefore the shapes have been slightly altered in Fig.5.

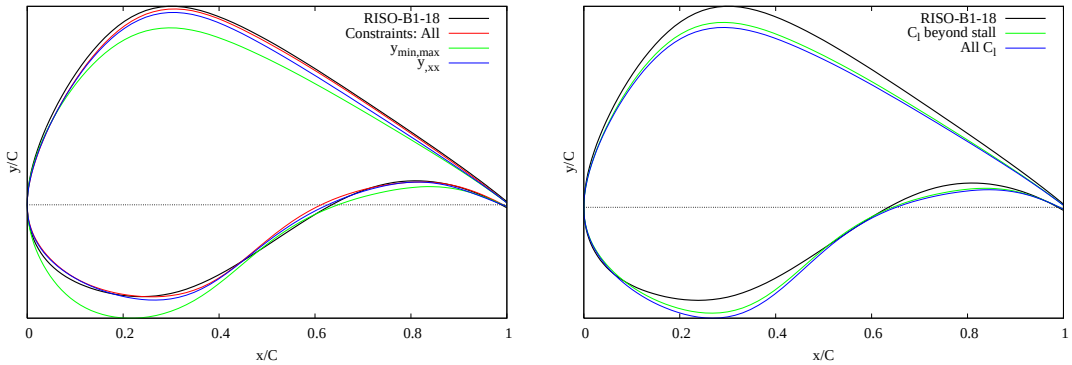

(a) Geometric Constraints (b) Aerodynamic Constraints

Figure 5: Airfoil Shapes after Optimization

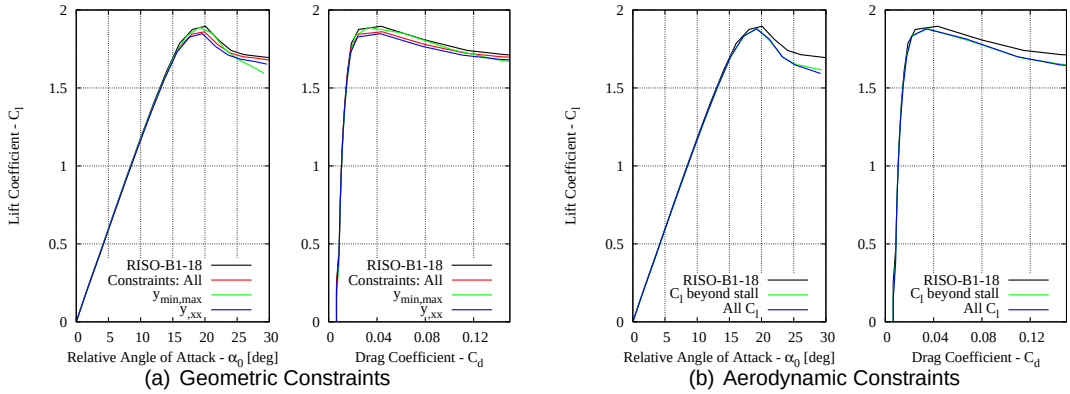

(a) Geometric Constraints (b) Aerodynamic Constraints

Figure 6: Aerodynamic Characteristics after Optimization (α_0)

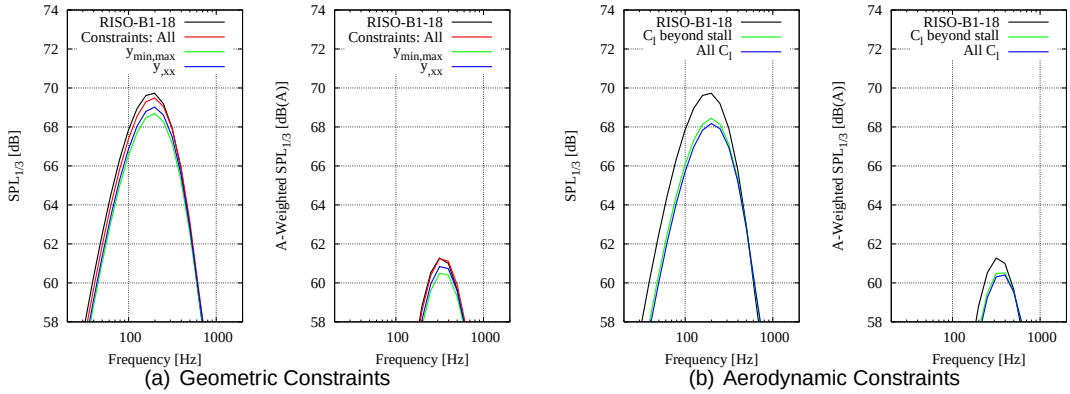

(a) Geometric Constraints (b) Aerodynamic Constraints

Figure 7: Far Field Noise after Optimization - $\alpha = 8^o$

3.4 Discussion

In order to get an insight into the design results, quantities relevant for trailing edge noise emission are compared before (i.e. for the RISØ-B1-18 airfoil) and after optimization. The optimized airfoil obtained with the "*All* C_l" set of constraints is considered here.

Fig.8(a) displays the velocity profiles across the boundary layer at several locations along the airfoil chord, the last one ($x/C = 0.975$) nearest to the trailing edge is used for trailing edge noise calculation. As it can be observed, the profiles are rather similar before and after optimization. The boundary layer thickness (evaluated by the extent of each curve on the y_2-axis, i.e. the distance to the wall) is neither significantly modified by the optimization procedure. Both boundary layer and momentum thicknesses on the suction side, the latter being more physically characteristic for trailing edge noise [11], along the airfoil chord are plotted on Fig.8(c). There are again rather small differences between the original and optimized design. As a last comparison, the Turbulent Kinetic Energy (TKE) profiles across the boundary layer are plotted at several chordwise positions in Fig.8(b). TKE directly relates to trailing edge noise through the vertical velocity turbulent shear stress $\overline{u_2^2}$ in Equation (1). It is clearly observed that the TKE is reduced for the optimized design, in particular near the trailing edge.

In return, the price to pay for the achieved noise reduction is a reduced airfoil camber and increased surface curvature, which resulted in a more abrupt decrease of lift in deep stall.

The reduction in generated noise remains small (1 to 2 dB), but substantial enough to make a difference for wind turbine design. In addition, the A-weighted SPL show as well a reduction in emitted noise though to a slightly lower level due to the filtering.

Note that the previous study remains quite subjective since different constraints from the original design were relaxed but no consideration about the specific importance of each constraint was taken into account, as well as to which extend each constraint could be relaxed without compromising the structural or aerodynamic properties of the final wind turbine blade.

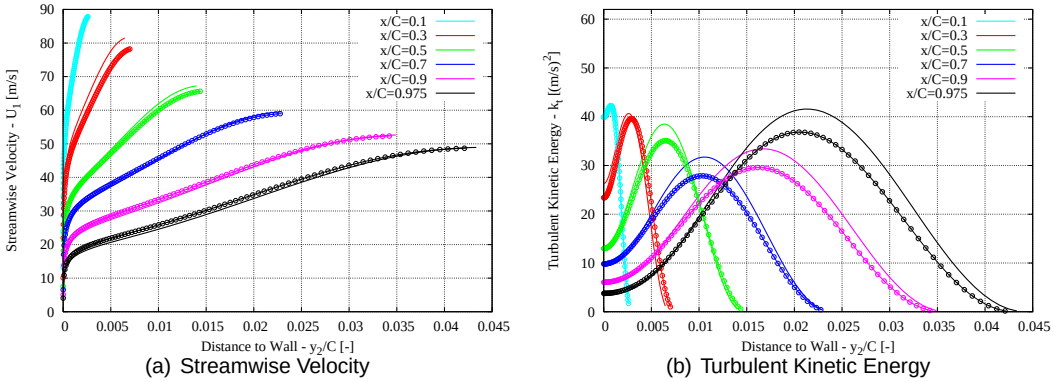

(a) Streamwise Velocity

(b) Turbulent Kinetic Energy

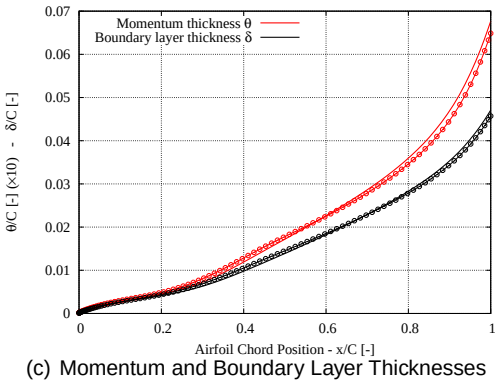

(c) Momentum and Boundary Layer Thicknesses

Figure 8: Boundary Layer Characteristics - $\alpha = 8^o$ (Lines: RISØ-B1-18 Airfoil; Lines with points: Optimized Airfoil ("*All* C_l")

4 Conclusions

In this paper, results obtained with the TNO trailing edge noise model for various test cases have been compared with experimental data. It was found in one case that the measured airfoil surface pressure were quite well predicted by the model. In two other cases, both the surface pressure and far field noise were largely underpredicted by the model, even though the tested airfoil and flow conditions didn't significantly differ with the previous case. However, the latter experiments were performed in wind tunnels designed for aeroacoustic measurements. The TNO model was still found reliable for relative comparisons and was used for aeroacoustically optimizing an existing airfoil. The noise emission could be reduced by 1 to 2 decibels. The noise reduction mechanism was found to be related to a reduction of the boundary layer turbulence intensity near the trailing edge. This was achieved by de-cambering the airfoil and the subsequent flattening of the suction side.

Acknowledgments

This work was sponsored by the Danish Energy Authorities within the Energy Research Project "Program for Research in Applied Aeroelasticity, EFP-2009". Computations were made possible by the use of the PC-clusters at the Risø central computing facility and the DCSC Center for Scientific Computing at DTU.

References

[1] Brooks TF, Pope SD, Marcolini MA, *Airfoil Self-Noise and Prediction*; Tech. Rep., NASA Reference Publication 1218, Langley Research Center, 1989.

[2] Amiet RK, Noise due to Turbulent Flow Past a Trailing Edge. *J. Sound Vib.* 1976; **47**(3):387-393.

[3] Fukano T, Kodama Y, Senoo Y, Noise Generated by Low Pressure Axial Flow Fans, I: Modeling of the Turbulent Noise. *J. Sound Vib.* 1977; **50**(1): 63-74.

[4] Parchen R, *Progress report DRAW: A Prediction Scheme for Trailing-Edge Noise Based on Detailed Boundary-Layer Characteristics*; TNO Rept. HAG-RPT-980023, TNO Institute of Applied Physics, The Netherlands, 1998.

[5] Blake WK, *Mechanics of Flow-Induced Sound and Vibration, Vol.I and II*; in Applied Mathematics and Mechanics, Frenkiel, F.N. and Temple, G. (eds.), Academic Press, 1986.

[6] Ffowcs Williams JE, Hall LH, Aerodynamic Sound Generation by Turbulent Flow in the Vicinity of a Scattering Half Plane. *J. Fluid Mech.* 1970; **40**(4):657-670.

[7] Howe MS, A Review of the Theory of Trailing Edge Noise. *J. Sound Vib.* 1978; **61**(3):437-465.

[8] Drela M, XFOIL: An Analysis and Design System for Low Reynolds Number Airfoils. *in Low Reynolds Number Aerodynamics, Mueller, T.J. (ed.), Lecture Notes in Engineering*; Springer-Verlag, Berlin, 1989; **54**:1-12.

[9] Moriarty P, Guidati G, Migliore P, Prediction of Turbulent Inflow and Trailing-Edge Noise for Wind Turbines. *AIAA Paper 2005-2881, Proc. of the* 11^{th} *AIAA/CEAS Aeroacoustics Conf.*, Monterey, 2005.

[10] Lutz T, Herrig A, Würz W, Kamruzzaman M, Krämer E, Design and Wind-Tunnel Verification of Low-Noise Airfoils for Wind Turbines. *AIAA Journal* 2007; **45**(4):779-785.

[11] Brooks TF, Hodgson TH, Trailing Edge Noise Prediction from Measured Surface Pressures. *J. Sound Vib.* 1981; **78**(1):69-117.

[12] Menter FR, Zonal Two-Equations $k-\omega$ Turbulence Models for Aerodynamic Flows. *AIAA Paper 93-2906*, 1993.

[13] Michelsen JA, *Block Structured Multigrid Solution of 2D and 3D Elliptic PDE's*; Tech. Rep. AFM 94-06, Technical University of Denmark, 1994.

[14] Sørensen NN, *General Purpose Flow Solver Applied to Flow over Hills*; PhD Thesis, Tech. Rep. Risø-R-827-(EN), Risø National Laboratory, Roskilde, Denmark, June 1995.

[15] Papenfuß HD, *Aerodynamic Commissioning of the New Wind Tunnel at LM Glasfiber A/S (Lunderskov)*; Private Communication, Institut für Thermo- und Fluiddynamik, Ruhr-Universität Bochum, Bochum, June 2006.

[16] Døssing M, *High Frequency Microphone Measurements for Transition Detection on Airfoils*; Tech. Rep. Risø-R-1645(EN), Risø-DTU, Roskilde, Denmark, 2008.

[17] Herr M, Design Criteria for Low-Noise Trailing-Edges. *AIAA Paper 2007-3470, Proc. of the* 13^{th} *AIAA/CEAS Aeroacoustics Conf.*, Rome, 2007.

[18] Humpf A, *Investigation of Computational Aeroacoustic Tools for Wind Turbine Aerofoils*; Diploma Thesis, CENER, Sarriguren, Spain, 2006.

[19] Kamruzzaman M, Lutz T, Herrig A, Krämer E, RANS Based Prediction of Airfoil Trailing Edge Far-Field Noise: Impact of Isotropic & Anisotropic Turbulence. *AIAA Paper 2008-2867, Proc. of the* 14^{th} *AIAA/CEAS Aeroacoustics Conf.*, Vancouver, 2008.

[20] Fuglsang P, Dahl KS, Multipoint Optimization of Thick High Lift Airfoil Wind Turbines. *Proc. EWEC'97*, Dublin, Ireland, 1997.

[21] Fuglsang P, Bak C. Development of the Risø Wind Turbine Airfoils. *Wind Energy* 2004; **7**:145-162.

[22] Fuglsang P, Bak C, Gaunaa M, Antoniou I, Design and Verification of the Risø-B1 Airfoil Family for Wind Turbines. *Journal of Solar Energy Engineering* 2004; **126**(4):1002-1010.